

Crystal structure and electromagnetic responses of tetragonal GdAlGe

Cong Wang(王聪), Yong-Quan Guo(郭永权)†, Tai Wang(王泰), and Shuo-Wang Yang(杨硕望)
Citation: Chin. Phys. B, 2020, 29 (**12**): 127502. DOI: 10.1088/1674-1056/abad25
Journal homepage: http://cpb.iphy.ac.cn; http://iopscience.iop.org/cpb

What follows is a list of articles you may be interested in

Anomalous Hall effect in ferromagnetic Weyl semimetal candidate $Zr_{1-x}V_xCo_{1.6}Sn$

Guangqiang Wang(王光强), Zhanghao Sun(孙彰昊), Xinyu Si(司鑫宇), Shuang Jia(贾爽)
Chin. Phys. B, 2020, 29 (**7**): 077503. DOI: 10.1088/1674-1056/ab8da8

Critical behavior in the layered organic-inorganic hybrid $(CH_3NH_3)_2CuCl_4$

Tina Raoufi, Yinina Ma(马怡妮娜), Young Sun(孙阳)
Chin. Phys. B, 2020, 29 (**6**): 067503. DOI: 10.1088/1674-1056/ab892c

Critical behavior and magnetocaloric effect in magnetic Weyl semimetal candidate $Co_{2-x}ZrSn$

Tianlin Yu(于天麟), Xiaoyun Yu(余骁昀), En Yang(杨恩), Chang Sun(孙畅), Xiao Zhang(张晓), Ming Lei(雷鸣)
Chin. Phys. B, 2019, 28 (**6**): 067501. DOI: 10.1088/1674-1056/28/6/067501

Influence of additives on the magnetic damping constant of CoIr soft magnetic thin films with negative magnetocrystalline anisotropy

Tianyong Ma(马天勇), Zhi Luo(罗智), Zhiwei Li(李志伟), Liang Qiao(乔亮), Tao Wang(王涛), Fashen Li(李发伸)
Chin. Phys. B, 2019, 28 (**5**): 057505. DOI: 10.1088/1674-1056/28/5/057505

Effects of chemical pressure on diluted magnetic semiconductor $(Ba,K)(Zn,Mn)_2As_2$

Y Peng(彭毅), S Yu(于爽), G Q Zhao(赵国强), W M Li(李文敏), J F Zhao(赵建发), L P Cao(曹立朋), X C Wang(望贤成), Q Q Liu(刘清青), S J Zhang(张思佳), R Z Yu(于润泽), Z Deng(邓正), X H Zhu(朱小红), C Q Jin(靳常青)
Chin. Phys. B, 2019, 28 (**5**): 057501. DOI: 10.1088/1674-1056/28/5/057501

Crystal structure and electromagnetic responses of tetragonal GdAlGe

Cong Wang(王聪), Yong-Quan Guo(郭永权)†, Tai Wang(王泰), and Shuo-Wang Yang(杨硕望)

School of Energy Power and Mechanical Engineering, North China Electric Power University, Beijing 102206, *China*

(Received 20 May 2020; revised manuscript received 20 July 2020; accepted manuscript online 7 August 2020)

The ternary rare-earth aluminum germanide GdAlGe with tetragonal structure is systematically studied by x-ray diffraction, magnetic and electric measurements. The magnetic and electric properties of GdAlGe are strongly related to its special magnetic structure formed by magnetic Gd3 isosceles triangles △s. The GdAlGe orders ferromagnetically at 21 K due to the exchanging interaction of Gd3 △↑-△↑ Gd3. The mechanism of magnetic transport originates from the slip scattering induced by Stoner spin fluctuation in the magnetic ordering region and the spin wave scattering induced by the thermal photon excitation and phonon scattering in the paramagnetic region. The positive magnetoresistance is observed in GdAlGe, which might be due to the disordered magnetic scatter induced by magnetic anisotropy in GdAlGe.

Keywords: GdAlGe, Weyl semimetal, magnetic isosceles triangle, electromagnetic response

PACS: 75.50.–y, 71.20.Eh, 75.60.Ej, 75.47.–m **DOI:** 10.1088/1674-1056/abad25

1. Introduction

Weyl fermions,[1] each of which consists of a pair of relativistic fermions with different chiralities, are originally considered as the particles in massless quantum electrodynamics, but they have not been observed as fundamental particles in nature. Although these conceptual fermions have been theoretically predicted in a framework of high energy physics, Weyl fermions are generally believed to be realized in the solid state, *i.e.* Weyl semimetals[2–10] type-I and type-II. Recently, it has been theoretically understood that the Weyl fermions can exist in some novel semimetals with non-trivial topology. However, the experimental study in this field has been held back because Weyl semimetals are extremely rare in nature. Although the quasiparticles in condensed matter systems can break Lorentz symmetry, the emergent Weyl fermions in the traditional (type-I) Weyl semimetal state,[11–14] which is realized in the TaAs class of materials,[15–19] still approximately complies with Lorentz symmetry. More recently, the so-called type-II[20–24] Weyl semimetal was proposed in WTe_2 material.[25–27] Though one is intensively interested in WTe_2 and it is one of various candidate materials, the type-II Weyl semimetal state is directly evidencd rarely in experiment until the recent direct observation of the type-II Weyl fermions in the nonmagnetic LaAlGe[28,29] based on angle resolved photo emission spectroscopic (ARPES) measurement, which paves the way for experimentally studying the novel spectroscopic and transport phenomena caused by the type-II Weyl fermions and provides a platform for testing the exotic Lorentz-violating high energy theories in table-top experiments. The mixture of Weyl semimetal, which includes type-I and type-II with inversion-breaking and time-reversal breaking, is proposed by the extensive study of *R*AlGe (*R* = La, Ce, Pr).[30] Thus, the interest has been extensively aroused in the family of *R*AlGe due to its remarkable tenability, depending on a suitable choice of rare earth elements. More recently, the crystal structure, magnetic anisotropy and magnetic transports have been experimentally studied on the predicted magnetic Weyl semimetals CeAlGe[31–33] and PrAlGe[33–35] single crystals. The CeAlGe orders antiferromagnetically at low temperatures and the PrAlGe shows a spin-glass-like characteristics at low temperatures. It is suggested that the GdAlGe be an antiferromagnetic (AFM) Weyl semimetal. However, the band structure has not been calculated due to the unmeasured detailed configuration of the AFM ordering in experiment.[30] The GdAlGe has two structures, *i.e.*, high temperature (HT) phase with tetragonal α-$ThSi_2$ type and low temperature (LT) phase with orthorhombic YAlGe type,[36,37] but there is no report on its properties, such as magnetic properties or electromagnetic responses. In this study, the crystal structure and electromagnetic responses of tetragonal GdAlGe are systematically studied for revealing the relation between the magnetoelectric properties and structure.

2. Experimental details

The raw metals of rare earth Gd, Ge, and Al with high purities more than 99.99 wt% were used for the sample preparation. The samples with normal structural formula of GdAlGe were prepared by using the non-consumable vacuum arc melting under atmosphere of high pure argon gas, and each sample was re-melted four times for ensuring the homogeneity. The

†Corresponding author. E-mail: yqguo@ncepu.edu.cn

© 2020 Chinese Physical Society and IOP Publishing Ltd

annealing process was carried out at 1373 K for 50 h in an evacuated quartz tube for eliminating the residual stress, and followed by quenching process in cooling water.

The crystal structures of samples were determined by powder x-ray diffraction (XRD) with Cu-$K_{\alpha 1}$ radiation. The diffraction peaks were initially indexed by Semi-Exhaustive Trial-and-Error (TREOR) program[38] for determining their lattice parameters and followed by structural refinement with the Rietveld powder diffraction profile fitting technique[39] for determining their crystal structures. The field emission scanning electron microscopy (SEM) equipped with energy dispersive x-ray spectroscopy (EDS) was used to check the chemical compositions. The applied field dependence of magnetization (M–H) and temperature dependence of magnetization (M–T) were measured by using a superconducting quantum interference device (SQUID)-vibrating sample magnetometer (VSM) in applied fields ranging from −50 kOe (1 Oe = 79.5775 A·m^{-1}) to 50 kOe at 5 K, 10 K, 15 K, 25 K for M–H measurement and in temperature ranging from 5 K to 300 K with applying external field of 100 Oe for M–T measurement. The temperature dependence of resistivity (R–T) was measured by using a physical property measurement system (PPMS) with a standard four-probe technique from 5 K to 300 K under an applied field of 50 kOe. The field dependence of magnetoresistance was investigated in fields ranging from −50 kOe to 50 kOe and at temperatures ranging from 5 K to 300 K.

3. Results and discussion

3.1. Crystal structure

The XRD phase identification, which is based on the International Center of Diffraction Database (ICDD), confirms that the annealed sample is single phase. Figure 1 shows the refined XRD patterns of GdAlGe, where the observed and calculated XRD patterns are marked with the symbol of "+" and solid lines, respectively. The lowest trace indicates the difference between the observed and calculated XRD patterns. The diffraction peaks are marked with Miller planar indices in the XRD pattern.

The determination of the crystal structure is first based on a structural model of isomorphic α-$ThSi_2$ with a space group of $I4_1/amd$ for the tetragonal phase according to Ref. [37], where the crystal positions are occupied by the rare earth Gd atoms at 4a site and Al/Ge at 8e site. However, this model does not fit the experimental XRD patterns well due to the high figural residual factor R and weighted figural residual factor R_{wp}, which originates from the disordered occupation of Al and Ge atoms at 8e, which is caused by the symmetric operation of a glide plane perpendicular to the c axis. If a glide plane is removed from the structural model, the space group is modified as $I4_1md$. This modified model has been successfully used to determine the crystal structure of LaAlGe,[28,29] CeAlGe,[31–33] and PrAlGe.[33–35] The essential difference between the two structural models is the atomic occupation transition from the disordered state at 8e site to the ordered state at two nonequivalent 4a sites for Al and Ge. The structural model with a space group of $I4_1md$ works for tetragonal GdAlGe, where the rare earth Gd, Al, and Ge occupy orderly three kinds of nonequivalent 4a sites with atomic ordinates (0, 0, 0.58854) for Gd, (0, 0, 0.14990) for Al and (0, 0, 0) for Ge, respectively. The lattice parameters of GdAlGe are $a = 4.1500$ Å and $c = 14.4033$Å. The structural refinement parameters of GdAlGe are listed in Table 1.

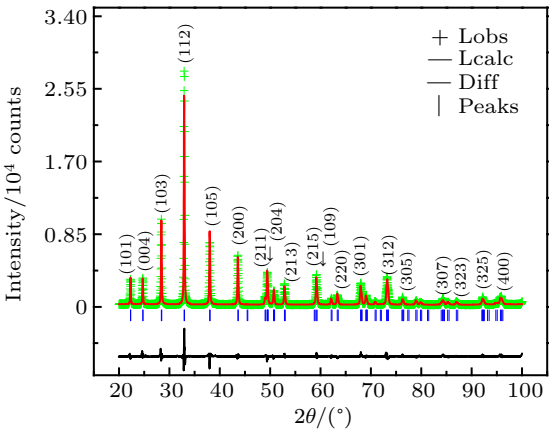


Fig. 1. Refined and observed XRD patterns of GdAlGe.

Table 1. Refined structure parameters of GdAlGe.

Parameters	Values
a/Å	4.1500
b/Å	4.1500
c/Å	14.4033
Gd 4a	(0,0,0.55854)
	N 4
Al 4a	(0,0,0.14990)
	N 4
Ge 4a	(0,0,0)
	N 4
R_p	7.534
R_{wp}	9.945
s	2.375

According to the refined crystallographic parameters, the tetragonal structure of GdAlGe can be constructed by using Diamond software as shown in Fig. 2. The crystal cell consists of alternating stack of A/B layers arranged by Ge3, Al3, and Gd3 isosceles triangle △ in the A layer/Gd3, Ge3, and Al3 reversed isosceles triangle ▽ in the B layer along the short edge direction (a axis). The symmetry along the long edge direction (c axis) shows that the unit cell is constructed by the trigonal prisms of Ge6, Al6, and Gd6 constructed by the isosceles

triangles △s between two A-layers, the Gd3, Ge3, and Al3 reversed isosceles triangles ▽s in the B layer and two layers of Ge4 squares □s. Based on the A/B stack, a nonsymmorphic C4 rotation symmetry is formed along the c-axial direction by shifting $c/4$, and this structure could give rise to Weyl fermions because of lack of space-inversion symmetry,[28] without symmetry center marked by symbol ⋆.

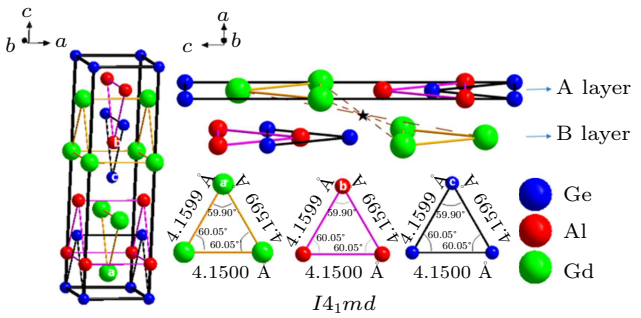


Fig. 2. Crystal structures of GdAlGe, where bond lengths and bond angles of isosceles triangles △ and ▽ formed by Gd, Al, Ge are supplied, double tetrahedron of Gd3 △ and ▽ Gd3 with common vertex marked with black star ⋆ is shown in tetragonal structure.

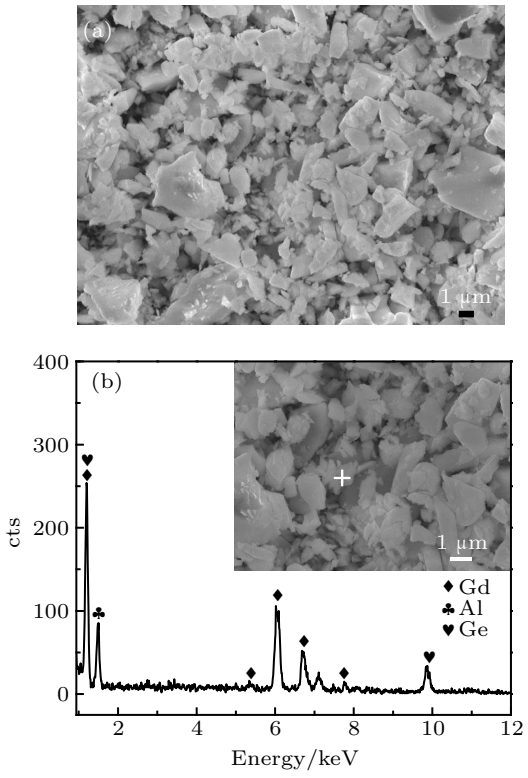


Fig. 3. SEM morphology and EDS pattern of GdAlGe.

Table 2. The quantitative atomic compositions in GdAlGe detected by EDS.

GdAlGe	Designed	Measurement
$[Gd_L]$/at.%	33.33	31.91
$[Al_K]$/at.%	33.33	34.25
$[Ge_K]$/at.%	33.33	33.85

The SEM morphology and EDS spectrum of GdAlGe are shown in Figs. 3(a) and 3(b), respectively. The grains are distributed irregularly with sizes ranging from 1 μm to 5 μm. The chemical compositions are listed in Table 2. The atomic ratio among Gd, Al and Ge is nearly 1:1:1. The content of Gd is slightly lower than that of the normal composition due to the evaporation in the melting preparation.

3.2. Magnetic properties

The GdAlGe orders ferromagnetically at 21 K as shown in Fig. 4. In general, the ferromagnetism can be explained as Zeeman coupling to the conduction electron states,[30] which lifts the spin degeneracy by time-reversal symmetry breaking and required Weyl semimetals. The temperature-dependent paramagnetic susceptibilities of tetragonal GdAlGe follows the Curie–Weiss law in the paramagnetic temperature region as shown in the inset of Fig. 4. According to the fitted Curie–Weiss constant, the effective magnetic moment $P_{\rm eff}$ of GdAlGe is estimated as 8.20 $\mu_{\rm B}$. Since $P_{\rm eff}$ is close to the theoretic moment 7.94 $\mu_{\rm B}$ of Gd^{3+}, the contribution to moment originates from Gd atoms. The surplus moment is attributed to the polarization of the 5d–6s conduction electrons,[40] which can bring the strong electronic interactions to the Weyl fermionic system, leading to the time-reversal breaking.

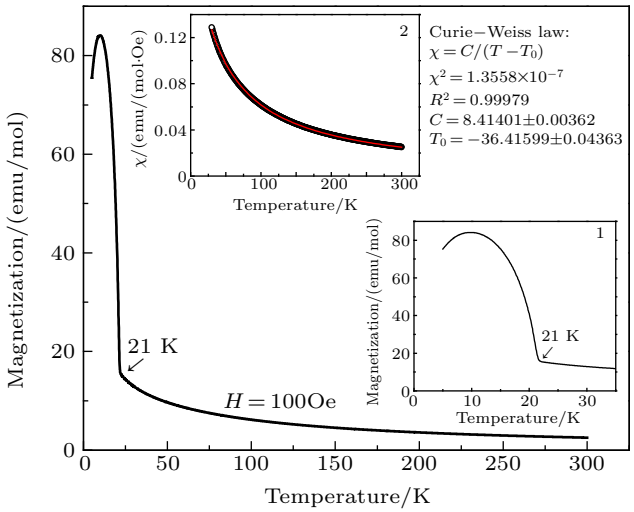


Fig. 4. Temperature-dependent magnetization for GdAlGe under applied field of 100 Oe, with insert plot 1 displaying enlarged M–T curve for showing clearly magnetic transition temperature, and insert plot 2 indicating observed and fitted M–T curve according to Curie–Weiss law in paramagnetic region.

It is suggested that the special structure of magnetic Gd3 isosceles triangle △ be strongly related to the magnetic response in GdAlGe. The magnetic order is related to the Gd3 △, the ferromagnetic order originates from the ferromagnetic exchanging interaction of Gd3 △↑-△↑ Gd3 between the two A layers. The field-dependent magnetizations for GdAlGe at various temperatures are studied and the results are shown in Fig. 5(a). The magnetization does not reach the saturation state under a maximum field of 50 kOe, which might be attributed to the magnetic structure of the strong magnetic anisotropy originating from the magnetic ordering arrangement of Gd atoms.

The same phenomena are observed in isostructural CeAlGe[31] and PrAlGe single crystals,[33] the easy magnetizing direction (EMD) and hard magnetizing direction (HMD) correspond to *a* axis and *bc* plane, the magnetization reaches saturation only along the EMD. The magnetization cannot reach the saturation along the HMD in a maximum applied field of 50 kOe. As for polycrystalline GdAlGe, the magnetizing process is disordered along various directions between EMD and HMD. Thus, it is difficult to reach the saturation state under an applied field of 50 kOe for the polycrystalline case. The magnetizing hysteresis loops of GdAlGe can be observed in the enlarged plot of Fig. 5(b) under the low field. The coercive force decreases from 0.24 kOe to 0.11 kOe with the temperature rising from 5 K to 25 K. However, the loop disappears at room temperature in the paramagnetic region.

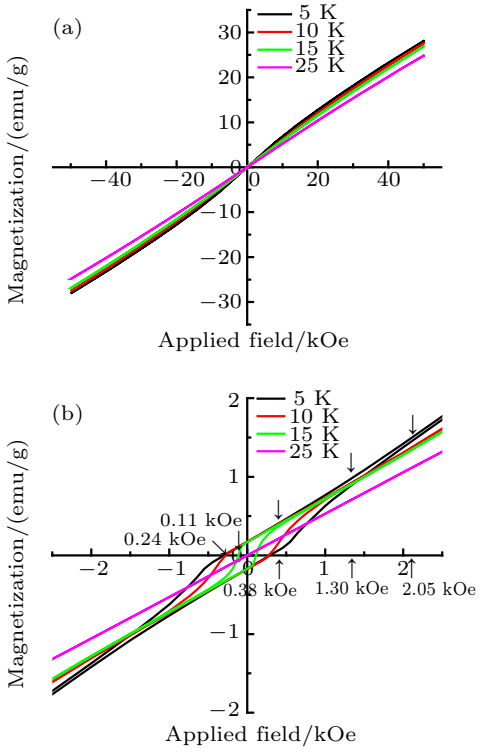


Fig. 5. Plots of (a) field-dependent magnetization and (b) its partial magnification indicating coercivity of GdAlGe at various temperatures.

3.3. Magnetic transport

The electric phase transitions are associated with the magnetic phase transitions in GdAlGe as shown in Fig. 6. Two electric phase transitions are observed: the one occurs at 21 K, which corresponds to Curie temperature T_c, implying that the electric transport is strongly related to the magnetic scattering interaction between spins of the conduction electrons and magnetic excitations such as Stoner fluctuations,[41] and the other one occurs at 51 K, which might be due to a superposition of different contributions in resistance: spin wave scattering induced by thermal excitation, phonon scattering, and spin flip scattering induced by the Stoner fluctuations. In the low temperature ferromagnetic region, the spin wave scattering caused by temperature-excited is forbidden, and since the energy of spin flip is lower than that of individual spin wave, the scattering caused by Stoner fluctuations effect preserves the conduction electrons spin.[42,43] The electric transport fits a semimetal power law model as follows:

$$\rho = \rho_{01} + a \cdot T^n, \tag{1}$$

where the first term on the right-hand side is the intrinsic resistivity, which is independent of temperature and magnetic property, and caused mainly by defects, electronic and nucleonic scattering;[44] the second term is most likely due to a spin flip scattering, where a and n denote the scattering coefficient and temperature indices, respectively. The scattering coefficient a reflects the spin flip scattering capability, and n is the temperature index and its value is 2 for the normal metal and less than 2 for the semimetal. In our case, the fitted resistivity is well consistent with the experimental one in the ferromagnetic region. The fitted index n is 1.51 ($1 < n < 2$), which confirms that the GdAlGe is semimetal and Stoner fluctuation exists in the ferromagnetic state.[41] Thus, the essential status of transport is corresponding to the ferromagnetic semimetal phase. In the paramagnetic region, the Stoner spin fluctuation is suppressed, and the spin wave scattering and phonon scattering contribute to the resistivity, which can be explained as a result of an extinction of a spin flip scattering mechanism in the high-temperature region. The resistivity also follows a modified semimetal model and is expressed as

$$\rho = \rho_{02} + b \cdot (T - T_0)^n, \tag{2}$$

where T_0 is a constant, which is close to the transition temperature: the introduction of T_0 reveals that the spin wave scattering contributes to the resistivity beyond the region of magnetic ordering; b is a scattering coefficient, which reflects the scattering capability of the thermal excited spin wave. The temperature-dependent resistivity curves are fitted before and after 51 K, respectively. The fitted resistivity accords with the experimental one very well, and the fitted T_0 is very close to the ferromagnetic transition temperature, demonstrating that the magnetic scattering mechanism disappears and spin wave scattering contributes to the resistivity in the temperature region of $T > T_0$. The temperature index n decreases from 1.75 to 0.78 with the transition occurring at 51 K, and electric resistivity *versus* temperature curve bends down toward the temperature axis after 51 K, but this transition point is not observed in the magnetization curve (M–T), which implies that the thermally excited spin wave scattering tends to be saturated and the phonon scattering mainly contributes to the resistivity.

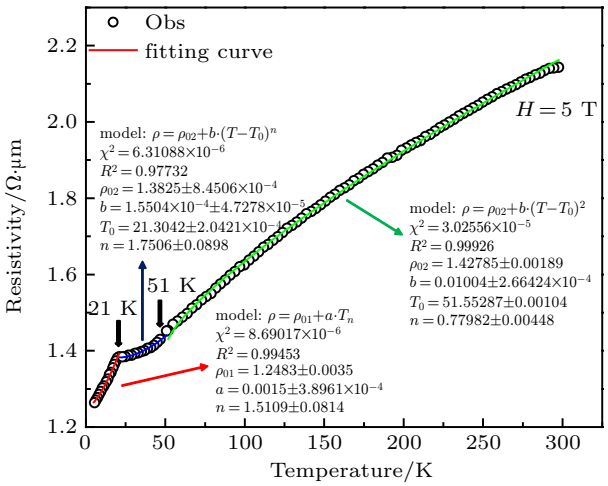


Fig. 6. Observed and fitted *R*–*T* curves for GdAlGe under applied field of 50 kOe.

The field-dependent resistances of GdAlGe are shown in Fig. 7(a). The resistance tends to increase with increasing applied field. The signals of measurement are very weak in a range from 0.00108 Ω and 0.00117 Ω, which causes the *R*–*H* curves to significantly fluctuate. The magnetoresistance (*MR*) equals the ratio between resistances before and after the application of external field as defined below:

$$MR = \frac{R(H) - R(0)}{R(0)}, \tag{3}$$

where $R(H)$ and $R(0)$ denote the resistances under an applied field of H and zero field, respectively. The magnetizing scattering contributes to *MR* and the relation between *MR* and magnetization (*M*) can be related by the following equation

$$MR = kM^2, \tag{4}$$

where k is a constant. The fitted *MR*–*H* curves of GdAlGe at various temperatures are shown in Fig. 7(b).

The weak positive *MR* with a maximum of 1.2% is obtained in the GdAlGe. The same phenomena are also observed in *R*AlGe (*R* = La, Ce)[31] and $ZrTe_5$[18] single crystals along the HMD (vertical to the *a* axis). The $ZrTe_5$ shows a large positive *MR* in the whole temperature range, which is different from the weak positive *MR* in GdAlGe. The Hall *MR* of TaAs is also positive along the field direction perpendicular to the current (equivalent to HMD). However, our interest focuses on the negative *MR*. No further explanation for the positive *MR* can be made. According to the quantum field theory, the occurring of Weyl points on Fermi level causes novel transport phenomenon related to the chiral anomaly,[45] such as the negative *MR* along the longitudinal direction (equivalent to EMD) under parallel electric and magnetic field.[46] The longitudinal negative *MR* arises from the non-zero Berry curvature of the Weyl fermions in TaAs. However, the *MR* is positive along the transversal direction.[45] In the case of GdAlGe, the magnetic anisotropy originates from the magnetization along the direction parallel or vertical to the special magnetic structure of Gd3 △↑-△↑ Gd3, which causes the magnetic scatterings different from electrons' scattering, and its *MR* should be corresponding to negative *MR* in EMD and positive *MR* in HMD. For polycrystalline GdAlGe, the magnetization is disordered along various directions between EMD (parallel to Gd3 △↑-△↑ Gd3) and HMD (vertical to Gd3 △↑-△↑ Gd3). The disordered magnetic scatters cause the resistance to increase and induce the positive *MR*. Thus, the *MR* of polycrystalline GdAlGe shows weak positive MR. It implies that the Weyl semimetal state exists only along the EMD in single crystal.

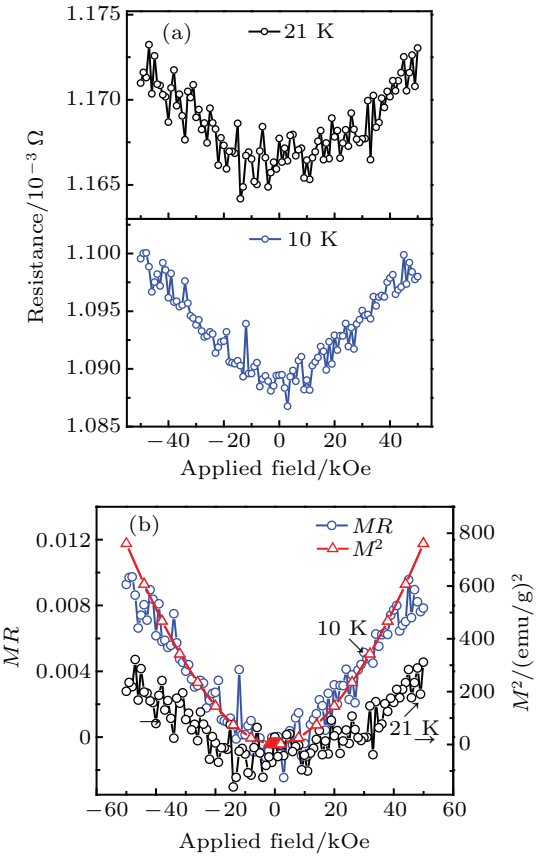


Fig. 7. Plots of (a) field-dependent resistance at 10 K and 21 K, and (b) magnetoresistances (*MR*s) of GdAlGe.

4. Conclusions

In this work, the proposed Weyl semimetal GdAlGe is systematically studied, which covers crystal structure, magnetic properties and magnetic transport. The space group of high-temperature phase GdAlGe is $I4_1md$, which is different from previously reported structure of α-$ThSi_2$ with a space group of $I4_1/amd$. The structural model changing from $I4_1/amd$ to $I4_1md$ is induced by the structural transition from disordered occupation (Al, Ge) at 8*e* site to the ordered oc-

cupations at two nonequivalent 4*a* sites for Al and Ge. The GdAlGe orders ferromagnetically at 21 K due to the exchange interaction of Gd3 △↑-△↑ Gd3 between two A-layers. The GdAlGe is hardly magnetized due to magnetic anisotropy, but the coercive force of GdAlGe decreases with temperature rising. The magnetic transport depends on the slip scattering induced by Stoner spin fluctuation in the magnetic ordering region and the spin wave scattering induced by thermal photon excitation and phonon scattering in the paramagnetic region. The positive *MR* is observed, which might be due to the disordered magnetic scatter induced by magnetic anisotropy in GdAlGe.

References

[1] Weyl H 1929 *Z. Phys.* **56** 330
[2] Belopolski I, Xu S Y, Sanchez D S, Chang G Q, Guo C, Neupane M, Zheng H, Lee C C, Huang S M, Bian G, Alidoust N, Chang T R, Wang B K, Zhang X, Bansil A, Jeng H T, Lin H, Jia S and Hasan M Z 2016 *Phys. Rev. Lett.* **116** 066802
[3] Burkov A A, Hook M D and Balents L 2011 *Phys. Rev. B* **84** 235126
[4] Chang M C and Yang M F 2015 *Phys. Rev. B* **91** 115203
[5] Inoue H, Gyenis A, Wang Z, Li J, Oh S W, Jiang S, Ni N, Bernevig B A and Yazdani A 2016 *Science* **351** 1184
[6] Jia S, Xu S Y and Hasan M Z 2016 *Nat. Mater.* **15** 1140
[7] Xu S Y, Belopolski I, Alidoust N, *et al.* 2015 *Science* **349** 613
[8] Weng H M, Dai X and Fang Z 2016 *J. Phys.: Condens. Matter* **28** 303001
[9] Bulmash D, Liu C X and Qi X L 2014 *Phys. Rev. B* **89** 081106(R)
[10] Wang G Q, Sun Z H, Si X Y, Jia S 2020 *Chin. Phys. B* **29** 077503
[11] Pavan H, Parameswaran S A and Ashvin V 2012 *Phys. Rev. Lett.* **108** 046602
[12] Li Q, Kharzeev D E, Zhang C, Huang Y, Pletikosić I, Fedorov A V, Zhong R D, Schneeloch J A, Gu G D and Valla T 2016 *Nat. Phys.* **12** 550
[13] Peng L, Zhang C H, Zhang J W, Yan W and Zhang X X 2018 *Phys. Rev. B* **98** 121108
[14] Burkov A A and Leon B 2011 *Phys. Rev. Lett.* **107** 127205
[15] Ma Q, Xu S Y, Chan C K, Zhang C L, Chang G Q, Lin Y X, Xie W W, Palacios T, Lin H, Jia S, Lee P, Herrero P J and Gedik N 2017 *Nat. Phys.* **13** 842
[16] Xu S Y, Alidoust N, Belopolski I, *et al.* 2015 *Nat. Phys.* **11** 748
[17] Lv B Q, Muff S, Qian T, Song Z D, Nie S M, Xu N, Richard P, Matt C E, Plumb N C, Zhao L X, Chen G F, Fang Z, Dai X, Dil J H, Mesot J, Shi M, Weng H M and Ding H 2015 *Phys. Rev. Lett.* **115** 217601
[18] Lv B Q, Xu N, Weng H M, Ma J Z, Richard P, Huang X C, Zhao L X, Chen G F, Matt C E and Bisti F 2015 *Nat. Phys.* **11** 724
[19] Huang S M, Xu S Y, Belopolski I, Lee C C, Chang G, Wang B K, Alidoust N, Bian G, Neupane M, Zhang C L, Jia S, Bansil A, Lin H and Hasan M Z 2015 *Nat. Commun.* **6** 7373
[20] Tamai A, Wu Q S, Cucchi I, Bruno F Y, Ricco S, Kim T K, Hoesch M, Barreteau C, Giannini E, Bernard C, Soluyanov A A and Baumberger F 2016 *Phys. Rev. X* **6** 031021
[21] Zyuzin A A and Tiwari R P 2016 *JETP Lett.* **103** 717
[22] O'Brien T E, Diez M and Beenakker C W 2016 *Phy. Rev. Lett.* **116** 236401
[23] Chang G Q, Xu S Y, Sanchez D S, Huang S M, Lee C C, Chang T R, Bian G, Zheng H, Belopolski I, Alidoust N, Jeng H T, Bansil A, Lin H and Hasan M Z 2016 *Sci. Adv.* **2** e1600295
[24] Zhu Z, Yan D, Nie X A, Xu H K, Yang X, Guan D D, Wang S Y, Li Y Y, Liu C H, Liu J W, Luo H X, Zheng H and Jia J F 2019 *Chin. Phys. B* **28** 077302
[25] Soluyanov A A, Gresch D, Wang Z, Wu Q S, Troyer M, Dai X and Bernevig A 2015 *Nature* **527** 495
[26] Ali M N, Jun X, Steven F, Jing T, Gibson Q D, Schoop L M, Tian L, Neel H, Max H, Ong N P and Cava R J 2014 *Nature* **514** 205
[27] Wu Y, Mou D X, Jo N H, Sun K W, Huang L N, Bud'ko S L, Canfield P C and Kaminski A 2016 *Phys. Rev. B* **94** 121113
[28] Xu S Y, Alidoust N, Chang G Q, *et al.* 2017 *Sci. Adv.* **3** e1603266
[29] Guloy A M and Corbett J D 1991 *Inorg. Chem.* **30** 4789
[30] Chang G Q, Singh B, Xu S Y, *et al.* 2018 *Phys. Rev. B* **97** 041104(R)
[31] Hodovanets H, Eckberg C J, Zavalij P Y, Kim H, Paglione J, Higgins J S and Paglione J 2018 *Phys. Rev. B* **98** 245132
[32] Suzuki T, Savary L, Liu J P, Lynn J W, Balents L and Checkelsky J G 2019 *Science* **365** 377
[33] Puphal P, Mielke C, Kumar N, Soh Y, Shang T, Medarde M, White J S and Pomjakushina E 2019 *Phys. Rev. Mater.* **3** 024204
[34] Meng B, Wu H, Qiu Y, Wang C L, Liu Y, Xia Z C, Yuan S L, Chang H X and Tian Z M 2019 *APL. Mater.* **7** 051110
[35] Yang H Y, Singh B, Lu B Z, Huang C Y, Bahrami F, Chu W C, Graf D, Huang S M, Wang B K, Lin H, Torchinsky D, Bansil A and Tafti F 2020 *APL Mater.* **8** 011111
[36] Pukas S, Lutsyshyn Y, Manyako M and Gladyshevskii E 2004 *J. Alloys Compd.* **367** 162
[37] Zhao J T and Parthé E 1990 *Acta Cryst.* **C46** 2276
[38] Werner P E, Eriksson L and Westdahl M J 1985 *J. Appl. Cryst.* **18** 367
[39] Rietveld H M 1969 *J. Appl. Cryst.* **2** 65
[40] Bozorth R M and Vleck J H V 1960 *Phys. Rev.* **118** 1493
[41] Guo Y Q and Li W 2007 *Appl. Phys. Lett.* **90** 042502
[42] Hordequin C, Pierre J and Currat R 1996 *J. Magn. Magn. Mater.* **162** 75
[43] Zhao G M, Smolyaninova V, Prellier W and Keller H 2000 *Phys. Rev. Lett.* **84** 6086
[44] Otto M J, Feil H, Woerden R A M V, Wijngaard J, Valk P J V D, Bruggen C F V and Haas C 1987 *J. Magn. Magn. Mater.* **70** 33
[45] Huang X C, Zhao L X, Long Y J, Wang P P, Chen D, Yang Z H, Liang H, Xue M Q, Weng H M, Fang Z, Dai X and Chen G F 2015 *Phys. Rev. X* **5** 031023
[46] Zhang C L, Xu S Y, Belopolski I, *et al.* 2016 *Nat. Commun.* **7** 10735